applied sciences

MDPI

Article

Multispectroscopic Study of Single Xe Clusters Using XFEL Pulses

Toshiyuki Nishiyama [1,2], Christoph Bostedt [3,4,5,6], Ken R. Ferguson [3], Christopher Hutchison [1], Kiyonobu Nagaya [1,2,*], Hironobu Fukuzawa [2,7], Koji Motomura [7], Shin-ichi Wada [8], Tsukasa Sakai [1], Kenji Matsunami [1], Kazuhiro Matsuda [1], Tetsuya Tachibana [7], Yuta Ito [7], Weiqing Xu [7], Subhendu Mondal [7], Takayuki Umemoto [8], Catalin Miron [9,10,11], Christophe Nicolas [9], Takashi Kameshima [12], Yasumasa Joti [12], Kensuke Tono [12], Takaki Hatsui [2], Makina Yabashi [2] and Kiyoshi Ueda [2,7]

1 Department of Physics, Kyoto University, Kyoto 606-8502, Japan; nishiyama.toshiyuki.68n@kyoto-u.jp (T.N.); chrisstopper@gmail.com (C.H.); tsukasa.sakai@hkt.muratec.co.jp (T.S.); matsunami.yaolab.kyoto@gmail.com (K.M.); matsuda.kazuhiro.5u@kyoto-u.ac.jp (K.M.)
2 RIKEN SPring-8 Center, Sayo, Hyogo 679-5148, Japan; fukuzawa@tohoku.ac.jp (H.F.); hatsui@spring8.or.jp (T.H.); yabashi@spring8.or.jp (M.Y.); kiyoshi.ueda@tohoku.ac.jp (K.U.)
3 Linac Coherent Light Source, SLAC National Accelerator Laboratory, Menlo Park, CA 94025, USA; christoph.bostedt@psi.ch (C.B.); kferguson@exponent.com (K.R.F.)
4 Chemical Sciences and Engineering Division, Argonne National Laboratory, 9700 S. Cass Avenue, Lemont, IL 60439, USA
5 Paul-Scherrer Institute, CH-5232 Villigen PSI, Switzerland
6 LUXS Laboratory for Ultrafast X-ray Sciences, Institute of Chemical Sciences and Engineering, École Polytechnique Fédérale de Lausanne (EPFL), CH-1015 Lausanne, Switzerland
7 Institute of Multidisciplinary Research for Advanced Materials, Tohoku University, Sendai 980-8577, Japan; motomura@spring8.or.jp (K.M.); tach.ymn@gmail.com (T.T.); y-ito@yz.yamagata-u.ac.jp (Y.I.); xuwq1@shanghaitech.edu.cn (W.X.); justsm@gmail.com (S.M.)
8 Department of Physical Science, Hiroshima University, Higashi-Hiroshima 739-8526, Japan; swada@sci.hiroshima-u.ac.jp (S.-i.W.); yggbyby@gmail.com (T.U.)
9 Synchrotron SOLEIL, l'Orme des Merisiers, Saint-Aubin, BP 48, 91192 Gif-sur-Yvette CEDEX, France; catalin.p.miron@gmail.com (C.M.); christophe.nicolas@synchrotron-soleil.fr (C.N.)
10 Extreme Light Infrastructure-Nuclear Physics (ELI-NP), "Horia Hulubei" National Institute for Physics and Nuclear Engineering, 30 Reactorului Street, Măgurele, RO-077125 Jud. Ilfov, Romania
11 Laboratoire Interactions, Dynamiques et Lasers (LIDYL), Commissariat à l'Energie Atomique et aux Energies Alternatives (CEA), Centre National de la Recherche Scientifique (CNRS), Université Paris-Saclay, CEA Saclay, 91191 Gif-sur-Yvette, France
12 Japan Synchrotron Radiation Research Institute (JASRI), Sayo, Hyogo 679-5198, Japan; kameshima@spring8.or.jp (T.K.); joti@spring8.or.jp (Y.J.); tono@spring8.or.jp (K.T.)
* Correspondence: nagaya.kiyonobu.3r@kyoto-u.ac.jp

Received: 19 October 2019; Accepted: 14 November 2019; Published: 16 November 2019

Abstract: X-ray free-electron lasers (XFELs) deliver ultrashort coherent laser pulses in the X-ray spectral regime, enabling novel investigations into the structure of individual nanoscale samples. In this work, we demonstrate how single-shot small-angle X-ray scattering (SAXS) measurements combined with fluorescence and ion time-of-flight (TOF) spectroscopy can be used to obtain size- and structure-selective evaluation of the light-matter interaction processes on the nanoscale. We recorded the SAXS images of single xenon clusters using XFEL pulses provided by the SPring-8 Angstrom compact free-electron laser (SACLA). The XFEL fluences and the radii of the clusters at the reaction point were evaluated and the ion TOF spectra and fluorescence spectra were sorted accordingly. We found that the XFEL fluence and cluster size extracted from the diffraction patterns showed a clear correlation with the fluorescence and ion TOF spectra. Our results demonstrate the effectiveness of the multispectroscopic approach for exploring laser–matter interaction in the X-ray regime without the influence of the size distribution of samples and the fluence distribution of the incident XFEL pulses.

Keywords: XFEL; diffractive imaging; fluorescence spectroscopy; ion spectroscopy

1. Introduction

The development of free-electron lasers (FEL) has enabled novel studies into the structure and dynamics of various forms of matter under extreme conditions, ranging from atoms and molecules [1–4] to condensed matter [5–7]. A particular interesting research field is the ultrafast dynamics of nanoscale samples triggered by intense FEL pulses, which provide basic insights into the mechanism of the laser–matter interaction. Atomic clusters are an ideal model system for this research. Their size is tunable and they are isolated systems with bulk density. The properties and responses of clusters in intense fields have been widely studied experimentally—using methods including charged-particle spectroscopy [8–17], X-ray diffraction [18–26], and fluorescence spectroscopy [27,28]—as well as theoretically [29–32].

Early experimental studies started with ion spectrometry, from which, unexpected energetic ion emissions, even in the short wavelength (extreme ultraviolet to X-ray) regime, were reported [9]. This stimulated discussion regarding the dynamics in clusters based on the spectra obtained by averaging over the ensemble of shots of the incident laser pulses. Pioneering works [18,22,33,34] revealed that the properties of individual particles are concealed by the accumulation of spectra due to the laser profile and to the size distribution and structural isomers of clusters originating from the generation methods.

X-ray free-electron laser (XFEL) sources provide a new pathway for the analysis of the structure of single particles. Intense and short X-ray pulses delivered from XFELs allow for the investigation of the structure of nanoscale samples and biomolecules [35,36] in the particle-by-particle regime, based on the diffraction before destruction scheme [37]. The structural analysis of free-flying clusters has been demonstrated by single-shot diffraction experiments [18–21,23,24,32]. The combination of single-shot imaging with spectroscopy allows for the studies of the laser–matter interaction, where experimental parameters such as the size and structure of the single particle target and the intensity of the irradiated laser pulses at the interaction point can be determined as additional parameters for the data analysis. This selective multispectroscopy has recently been proven to be valid in studies using the combination of small-angle X-ray scattering (SAXS) with ion spectroscopy [18,22]. In these studies, the characteristic and systematic structural ion spectra were specified by filtering the sample size and the intensity of XFEL pulses.

In this work, we present results of enhanced multispectroscopic measurements with XFEL pulses. We recorded SAXS signals from Xe clusters in combination with ion time-of-flight (TOF) spectra and fluorescence spectra for every XFEL pulse. We observed clear diffraction patterns from Xe clusters and extracted both the XFEL fluence at the actual interaction point and the cluster size from them. We found that the XFEL fluence and the cluster size had a clear correlation with the fluorescence and ion TOF spectra. Our results on the fluence dependence of the maximum charge state and the mean charge state of Xe ions in the hard X-ray regime are in good agreement with preceding works in the soft X-ray and ultraviolet spectral regime [18,22].

2. Materials and Methods

The experiment was carried out at the experimental hutch 3 of beamline 3 at the SACLA XFEL [38]. The details of the experimental setup have been described in detail elsewhere [39]; thus, we only summarize the experimental conditions briefly. A schematic of the experimental setup is shown in Figure 1. The wavelength of the XFEL was 2.2 Å (corresponding to a photon energy of 5.5 keV). The XFEL pulses were focused with a Kirkpatrick–Baez (KB) mirror system to a focal spot size of 1.5×1.3 μm^2 (full width at half maximum). The average peak fluence of the XFEL pulses during the measurements, J_0, was determined to be approximately 16 μJ/μm^2. The stray light from the KB mirror system was reduced using a 0.3×0.3 mm square aperture in a 0.5 mm tungsten plate,

installed 200 mm upstream of the interaction point. Xe clusters were prepared by expanding Xe gas adiabatically through a pulsed valve equipped with a convergent–divergent nozzle with a diameter of 200 µm and a half angle of 4°. The stagnation pressure P_0 and temperature T_0 were 21 bar and 300 K, respectively. For the experiments, we used extremely large clusters by timing the valve closure to the after-pulses as described in detail by Rupp et al. [23]. The shot-by-shot scattering signals were recorded using an octal multiport charge-coupled device (MPCCD) sensor [40]. The detector covered a scattering angle range of 0.10–2.8°, which corresponds to a momentum transfer of q = 0.049–1.4 nm^{-1}. In coincidence with each scattering signal, the fluorescence photons from the clusters were detected with two MPCCD single sensors set in the plane determined by the directions of XFEL and cluster pulses. Be windows separated the sensors from the main chamber. The ions were extracted with a TOF spectrometer equipped with microchannel plates and a delay-line anode (Roentdek HEX 80) [3].

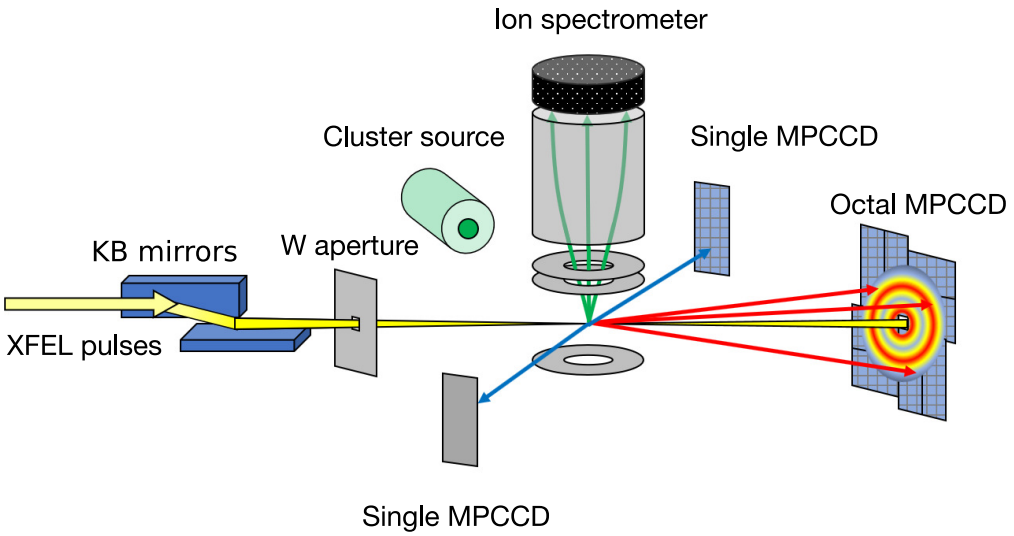

Figure 1. Schematic of the experimental setup. X-ray free-electron laser (XFEL) pulses were focused by a pair of Kirkpatrick–Baez (KB) mirrors. The cluster beam was generated through adiabatic expansion and introduced through two skimmers to the reaction point. The scattered photons were collected by an octal multiport charge-coupled device (MPCCD) sensor installed 1.5 m from the reaction point in the direction of XFEL beam. Fluorescence photons were detected by two single MPCCD sensors, whose distances from the reaction point were 0.6 m and 0.8 m, respectively. Ions were collected by an ion time-of-flight (TOF) spectrometer, set on the upper side of the chamber.

3. Results and Discussion

Figure 2 shows examples of SAXS images, fluorescence spectra, and ion TOF spectra from Xe clusters recorded in coincidence for each FEL pulse. Under our experimental conditions, the hit rate determined by the ratio of observed SAXS signals in the octal MPCCD sensor to the total number of FEL shots was less than 0.1%. Therefore, the recorded data of each FEL shot were considered to originate from a single cluster in the focus of the FEL pulse. In the SAXS images, we observed clear concentric diffraction rings which suggest a spherical shape of the Xe clusters. We analyzed the SAXS images with respect to the size of the Xe clusters as well as the fluence of XFEL pulses at the actual interaction point, described in detail in the following section. The obtained values of cluster size and XFEL fluence are summarized below in the panels (a), (d), and (g) in Figure 2. Further, Figure 2a–c shows the SAXS, fluorescence, and TOF spectra recorded at the highest fluence. Here, the diffraction pattern had a high intensity. The fluorescence spectrum shows an evident peak at around 5 keV, at the high energy side of the dark signal peak of the MPCCD sensor around 0 keV. Highly-charged ions were observed in the TOF spectrum. As the XFEL fluence decreased, as shown in Figure 2d–i, the SAXS signals got weaker, the yield of fluorescence photons decreased, and less highly charged

ions were observed, while ions in the lower charge state appeared more prominently. These results indicate that XFEL–cluster interaction can be studied more accurately using size- and fluence-selective measurements, i.e., by eliminating the washout of characteristics of single targets due to their size distribution and laser profile [18,22,33,34].

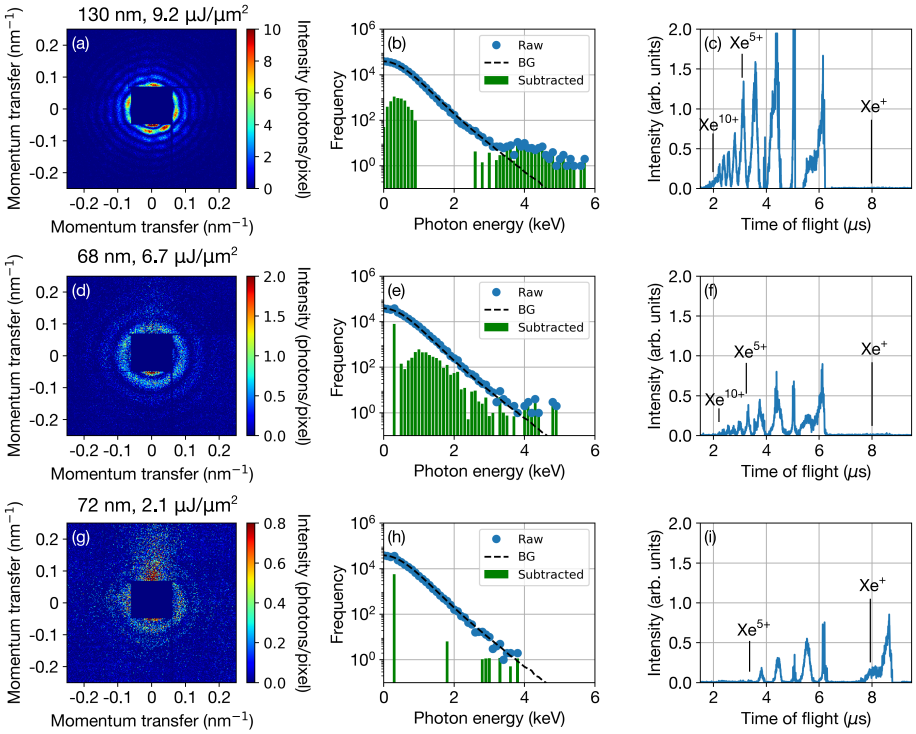

Figure 2. Characteristic results of the multispectroscopic measurements. Each diffraction image, fluorescence spectrum, and ion TOF spectrum shown in (**a**–**c**), (**d**–**f**), and (**g**–**i**) are observed from Xe clusters with the radii of cluster and the fluence (r_0, J_0) of (130 nm, 9.2 μJ/μm^2), (68 nm, 6.7 μJ/μm^2), and (72 nm, 2.1 μJ/μm^2), respectively. Scattered intensity was observed in the upper region of the diffraction images (**a**,**d**,**g**), which came from the parasitic scattering of the XFEL pulses due to the configuration of the upstream optical system.

3.1. Analysis of Small-Angle X-ray Scattering Data

The majority of the observed SAXS images exhibited concentric rings suggesting spherically shaped clusters. Additionally, we observed a few images indicating nonspherical clusters under the present conditions [41], as reported in the preceding works [20,21,23]. For the concentric ring SAXS images, we deduced both the radii of clusters and XFEL fluences by assuming a single uniformly dense sphere. It is noted that the absorption efficiency of 5.5 keV photons by a Xe atom is very low and the scattering from electrons bound to Xe atoms can be expressed by Thomson scattering [42]. In the regime of infrared to soft X-ray, the scattering is well described by Mie scattering [43], where the absorption efficiency of a Xe atom is much higher [20]. Figure 3a shows the typical radial profiles derived from diffraction images and the corresponding fitting curves. The fits, assuming a single uniformly dense sphere and Thomson scattering, reproduced the experimental results well. Figure 3b shows the histogram of radii of the observed Xe clusters and a curve (black dotted line) describing a log-normal distribution of the cluster size. The cluster radii peaked around 70 nm, but also much larger clusters were observed. The large cluster's radii go well beyond the well-known scaling law [44,45] (25–44 nm) as a result of our specific experimental conditions, i.e., timing the jet to an after pulse to generate extremely large clusters [23].

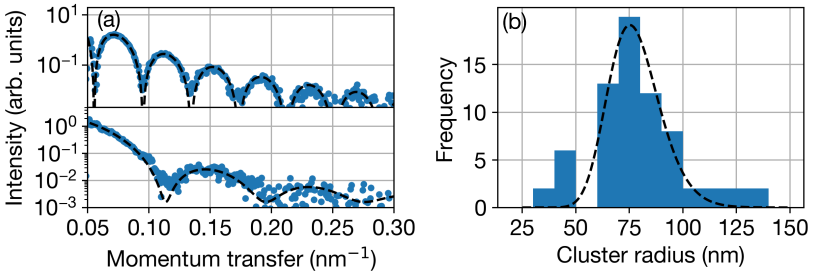

Figure 3. (**a**) Characteristic radial profiles of diffraction images. The radii of the Xe clusters giving the top and bottom and the profiles are 81 nm and 39 nm, respectively. The formula of the fitting curves (black dotted lines) is described in [39]. (**b**) The histogram of radii of the observed Xe clusters. The black dotted line is a fitting curve based on the log-normal distribution of cluster size and gives the average radius of 80 nm.

3.2. Fluorescence Spectroscopy

We evaluated the energy and the number of fluorescence photons coming from Xe clusters for the spectra shown in Figure 2b,e,h. Under conditions where the intensity of the incident beam is not extremely high, the number of fluorescence photons from a cluster, N_{flu}, can be assumed to be proportional to the product of J_0 and the cluster volume, i.e., the number of atoms in the cluster N ($\propto r_0^3$). On the other hand, the number of scattered photons, N_{scat}, is proportional to the product of J_0 and $N^{4/3}$ ($\propto r_0^4$) considering spherical shaped clusters. Therefore, one can expect a relation between N_{flu} and N_{scat} as $N_{flu} \times r_0 \propto N_{scat}$. We extracted the number of fluorescence photons from xenon clusters by subtracting the background signals in the fluorescence spectra. We also estimated N_{scat} from SAXS data, and checked the correlation between $N_{flu} \times r_0$ and N_{scat}, as shown in Figure 4a. In Figure 4a, there is evidence of a linear correlation between N_{scat} and $N_{flu} \times r_0$, indicating that the observed fluorescence and scattering photons came from the same targets for each XFEL shot. We also plotted the position of the fluorescence photon peak in Figure 4b. A broad peak was found to be located at 4 keV; the position of this peak was not changed by the FEL fluence. The observed peak position corresponds to the fluorescence energies of the Xe atomic L_α and L_β lines. Therefore, these photons are a result of the radiative decay of inner-core excited Xe atoms in the cluster. These results show that fluorescence spectroscopy monitoring of the fluence of the incident pulses offers the possibility of studying the degree of inner ionization of samples under an intense laser field [5,6,28,46].

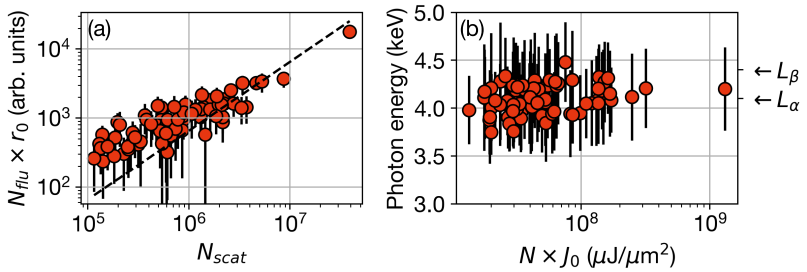

Figure 4. Correlation maps between the observables obtained from fluorescence spectrum and small-angle X-ray scattering (SAXS). (**a**) Correlation between the number of scattered photons detected by the octal MPCCD and fluorescence photons detected by one of the two single MPCCD sensors. The black dotted line is a guide representing $N_{flu} \times r_0 \propto N_{scat}$. (**b**) Correlation between the X-ray dose (=cluster size $\times$ XFEL fluence) and the photon energy of fluorescence. The positions of the photon energies of Xe atomic L_α and L_β fluorescence are shown to the right side of (**b**). The error bars shown in both (**a**,**b**) are composed of the statistical errors of the number of fluorescence photons.

3.3. Ion TOF Spectroscopy

Figure 5 shows ion TOF spectra of Xe clusters taken under different conditions for high FEL fluences (∼8 μJ μm^{-2}) in panels (a)–(c) and low FEL fluences (∼3 μJ μm^{-2}) in panels (d)–(f), respectively. The charge distributions of the detected ion yields extracted from each TOF spectrum are shown in the insets of each ion TOF spectrum. Substantial TOF intensity of singly charged Xe ions was observed at a lower XFEL fluence irrespective of cluster size. On the other hand, singly charged ions were suppressed and more highly charged ions were generated at higher XFEL fluence. To investigate the dependence of the charge state on other observables, the maximum charge state and the average charge state were extracted from each TOF spectrum.

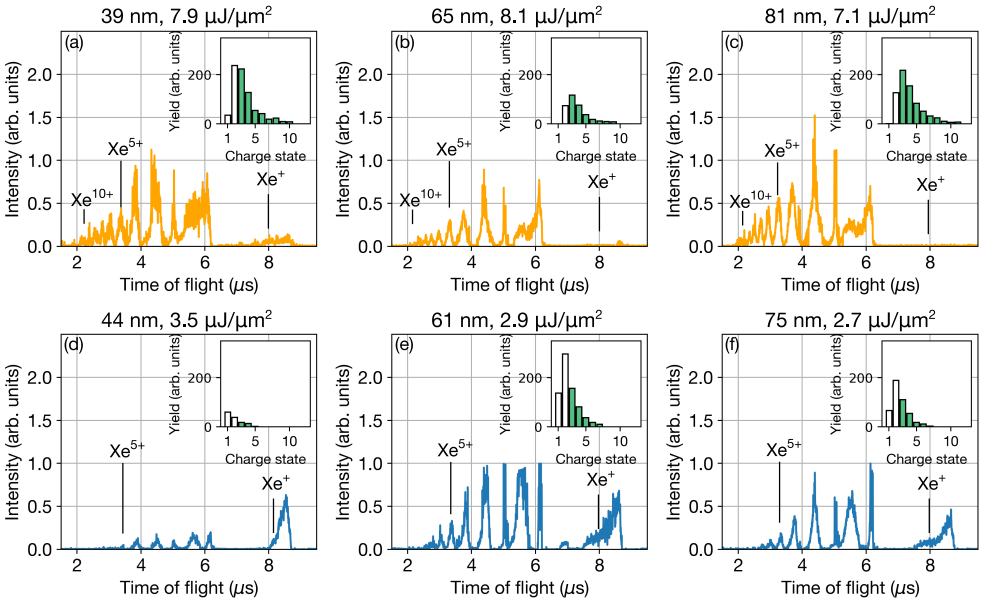

Figure 5. Ion TOF spectra of Xe clusters with sizes of approximately (**a**,**d**) 40 nm, (**b**,**e**) 60nm, and (**c**,**f**) 80 nm. TOF spectra observed for high FEL fluences (∼8 μJ μm^{-2}) are shown in (**a**–**c**) , and those observed for low FEL fluences (∼3 μJ μm^{-2}) are shown in (**d**–**f**). Ion charge states of each peak were determined by a simulation using SIMION [47]. The charge distributions of the detected Xe ions extracted from each TOF spectrum are shown in the insets. The yields of doubly charged ions and singly charged ions are less reliable due to the lowering of detection efficiency and the saturation of the signal, which were caused by the detection of a large number of highly charged Xe ions. The baseline of spectra is corrected because it was modulated due to the lowering of detection efficiency and the detection of a large number of ions.

Figure 6a,b show the XFEL fluence dependence of the maximum charge state (Z_{max}) and the apparent averaged charge state (Z_{ave}) of Xe ions. Z_{max} increased steeply and saturated at around 12 as the XFEL fluence increased. Z_{ave} also increased with the XFEL fluence. In the current data set, both Z_{max} and Z_{ave} seemed to show a slight dependence on the cluster size, but further discussion regarding the size dependence is difficult because there are limited data. Elucidation of the size dependence is an important theme for furthering our understanding of the laser–matter interaction.

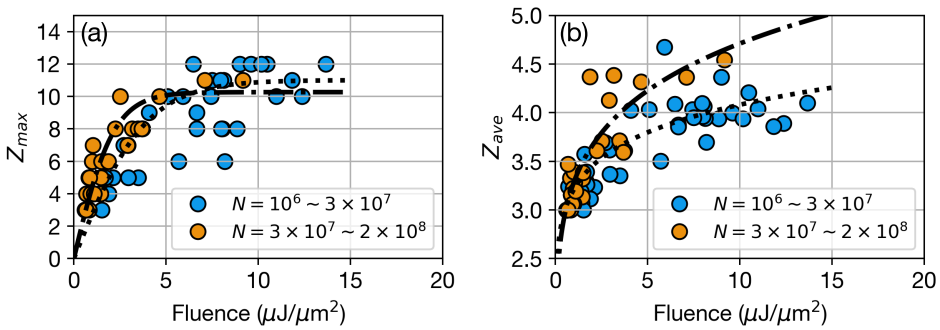

Figure 6. XFEL fluence dependence on the charge state of Xe ions. (**a**) The observed maximum charge state Z_{max}. (**b**) The apparent averaged charge state Z_{ave} calculated by weighted averaging over the peaks in the TOF spectrum corresponding to the charge state $\geq$3. The dashed lines and the dotted lines in (**a**,**b**) are the guides for the eyes.

The strong dependence of the charge state of Xe ions on the fluence of the XFEL pulses is in agreement with the preceding studies using soft XFELs with 91 eV [18] and 800 eV [22]. Moreover, the suppression of singly charged ions and the steep increase in charge state with higher fluence also agrees well with the results using 800 eV XFEL pulses [22], suggesting the efficient suppression of electron–ion recombination. Notably, the saturated charge state observed in this study was also lower compared to the preceding studies. This difference may be due to the different excitation energy, deposition energy, and ionization efficiency of the incident photons.

4. Conclusions

We carried out multispectroscopic measurements of single Xe clusters at SACLA. The SAXS signals, fluorescence spectra, and ion TOF spectra of giant xenon clusters were recorded simultaneously on a shot-by-shot basis. The radii of the clusters and the XFEL fluences at the reaction point were evaluated from SAXS data, and the ion TOF spectra and fluorescence spectra were sorted according to the obtained parameters. After sorting, we found a clear size and FEL fluence dependence in both the ion TOF and fluorescence spectra. The present results demonstrate the importance of removing the averaging effects of the size distribution of the clusters as well as the laser fluence profile to obtain deep insights into the laser–matter interaction. The information extracted from our single-shot single-particle data sets, the first in the hard X-ray regime and the first containing inner-shell fluorescence information, is in good agreement with the findings of previous studies using similar styles of single-shot approaches in the soft X-ray and ultraviolet spectral regime. Our work underlines the potential of size- and fluence-selective spectroscopy for advancing the research in laser–matter interaction.

Author Contributions: Conceptualization, K.N. and K.U.; data curation, T.N., C.H., W.X., T.S., K.M. (Kenji Matsunami), T.T. and S.M.; formal analysis, T.N.; funding acquisition, W.X.; investigation, T.N., C.B., K.R.F., C.H., K.N., H.F., K.M. (Koji Motomura), S.-i.W., T.S., K.M. (Kenji Matsunami), K.M. (Kazuhiro Matsuda), T.T., Y.I., W.X., S.M., T.U., C.N., C.M., T.K., Y.J., K.T., T.H., M.Y. and K.U.; methodology, T.N., K.N., H.F.; project administration, C.B., K.N. and K.U.; resources, T.N., C.B., K.N., S.-i.W., T.S. and K.M. (Kenji Matsunami); software, T.N., C.H., and K.M. (Koji Motomura); supervision, K.N. and K.U.; validation, T.N., K.N. and K.U.; visualization, T.N. and K.N.; writing—original draft preparation, T.N. and K.N.; writing—review and editing, K.N., C.M., and C.B.

Funding: This research was supported by the National Nature Science Foundation of China (Grant No. 11604003).

Acknowledgments: We are grateful to the late Makoto Yao for his invaluable contributions to the present work. The XFEL experiments were performed at the BL3 of SACLA with the approval of the Japan Synchrotron Radiation Research Institute (JASRI) and the program review committee (2014A8038). This study was supported by the X-ray Free Electron Laser Utilization Research Project and the X-ray Free Electron Laser Priority Strategy Program of the Ministry of Education, Culture, Sports, Science and Technology of Japan (MEXT), by the Japan Society for the Promotion of Science (JSPS), by the Proposal Program of SACLA Experimental Instruments of RIKEN, by the IMRAM project, and by the Cooperative Research Program, the Research Program for Next Generation Young Scientists of "Network Joint Research Center for Materials and Devices: Dynamic Alliance for Open Innovation

Bridging Human, Environment and Materials". C.B. and K.R.F. acknowledge support from the U.S. Department of Energy, Office of Basic Energy Sciences, Division of Chemical Sciences, Geosciences, and Biosciences through SLAC and Argonne National Laboratories.

Conflicts of Interest: The authors declare no conflict of interest.

References

1. Young, L.; Kanter, E.P.; Krässig, B.; Li, Y.; March, A.M.; Pratt, S.T.; Santra, R.; Southworth, S.H.; Rohringer, N.; DiMauro, L.F.; et al. Femtosecond electronic response of atoms to ultra-intense X-rays. *Nature* **2010**, *466*, 56–61. [CrossRef] [PubMed]
2. Rudek, B.; Son, S.-K.; Foucar, L.; Epp, S.W.; Erk, B.; Hartmann, R.; Adolph, M.; Andritschke, R.; Aquila, A.; Berrah, N.; et al. Ultra-efficient ionization of heavy atoms by intense X-ray free-electron laser pulses. *Nat. Photonics* **2012**, *6*, 858–865. [CrossRef]
3. Motomura, K.; Fukuzawa, H.; Son, S.-K.; Mondal, S.; Tachibana, T.; Ito, Y.; Kimura, M.; Nagaya, K.; Sakai, T.; Matsunami, K.; et al. Sequential multiphoton multiple ionization of atomic argon and xenon irradiated by X-ray free-electron laser pulses from SACLA. *J. Phys. B At. Mol. Opt. Phys.* **2013**, *46*, 164024. [CrossRef]
4. Erk, B.; Boll, R.; Trippel, S.; Anielski, D.; Foucar, L.; Rudek, B.; Epp, S.W.; Coffee, R.; Carron, S.; Schorb, S.; et al. Imaging charge transfer in iodomethane upon X-ray photoabsorption. *Science* **2014**, *345*, 288–291. [CrossRef]
5. Vinko, S.M.; Ciricosta, O.; Cho, B.I.; Engelhorn, K.; Chung, H.-K.; Brown, C.R.D.; Burian, T.; Chalupský, J.; Falcone, R.W.; Graves, C.; et al. Creation and diagnosis of a solid-density plasma with an X-ray free-electron laser. *Nature* **2012**, *482*, 59–62. [CrossRef]
6. Ciricosta, O.; Vinko, S.M.; Chung, H.-K.; Cho, B.-I.; Brown, C.R.D.; Burian, T.; Chalupský, J.; Engelhorn, K.; Falcone, R.W.; Graves, C.; et al. Direct Measurements of the Ionization Potential Depression in a Dense Plasma. *Phys. Rev. Lett.* **2012**, *109*, 065002. [CrossRef]
7. Tamasaku, K.; Shigemasa, E.; Inubushi, Y.; Katayama, T.; Sawada, K.; Yumoto, H.; Ohashi, H.; Mimura, H.; Yabashi, M.; Yamauchi, K.; et al. X-ray two-photon absorption competing against single and sequential multiphoton processes. *Nat. Photonics* **2014**, *8*, 313–316. [CrossRef]
8. Ditmire, T.; Donnelly, T.; Rubenchik, A.M.; Falcone, R.W.; Perry, M.D. Interaction of intense laser pulses with atomic clusters. *Phys. Rev. A* **1996**, *53*, 3379–3402. [CrossRef]
9. Wabnitz, H.; Bittner, L.; de Castro, A.R.B.; Döhrmann, R.; Gürtler, P.; Laarmann, T.; Laasch, W.; Schulz, J.; Swiderski, A.; von Haeften, K.; et al. Multiple ionization of atom clusters by intense soft X-rays from a free-electron laser. *Nature* **2002**, *420*, 482–485. [CrossRef]
10. Hoener, M.; Bostedt, C.; Thomas, H.; Landt, L.; Eremina, E.; Wabnitz, H.; Laarmann, T.; Treusch, R.; de Castro, A.R.B.; Möller, T. Charge recombination in soft X-ray laser produced nanoplasmas. *J. Phys. B At. Mol. Opt. Phys.* **2008**, *41*, 181001. [CrossRef]
11. Bostedt, C.; Thomas, H.; Hoener, M.; Eremina, E.; Fennel, T.; Meiwes-Broer, K.-H.; Wabnitz, H.; Kuhlmann, M.; Plönjes, E.; Tiedtke, K.; et al. Multistep Ionization of Argon Clusters in Intense Femtosecond Extreme Ultraviolet Pulses. *Phys. Rev. Lett.* **2008**, *100*, 133401. [CrossRef] [PubMed]
12. Iwayama, H.; Nagaya, K.; Yao, M.; Fukuzawa, H.; Liu, X-J.; Prümper, G.; Motomura, K.; Ueda, K.; Saito, N.; Rudenko, A.; et al. Frustration of photoionization of Ar nanoplasma produced by extreme ultraviolet FEL pulses. *J. Phys. At. Mol. Opt. Phys.* **2013**, *46*, 164019. [CrossRef]
13. Fukuzawa, H.; Son, S.-K.; Motomura, K.; Mondal, S.; Nagaya, K.; Wada, S.; Liu, X.-J.; Feifel, R.; Tachibana, T.; Ito, Y.; et al. Deep Inner-Shell Multiphoton Ionization by Intense X-ray Free-Electron Laser Pulses. *Phys. Rev. Lett.* **2013**, *110*, 173005. [CrossRef] [PubMed]
14. Schütte, B.; Arbeiter, M.; Fennel, T.; Vrakking, M.J.J.; Rouzée, A. Rare-Gas Clusters in Intense Extreme-Ultraviolet Pulses from a High-Order Harmonic Source. *Phys. Rev. Lett.* **2014**, *112*, 073003. [CrossRef]
15. Schütte, B.; Campi, F.; Arbeiter, M.; Fennel, T.; Vrakking, M.J.J.; Rouzée, A. Tracing Electron-Ion Recombination in Nanoplasmas Produced by Extreme-Ultraviolet Irradiation of Rare-Gas Clusters. *Phys. Rev. Lett.* **2014**, *112*, 253401. [CrossRef]
16. Kumagai, Y.; Jurek, Z.; Xu, W.; Fukuzawa, H.; Motomura, K.; Iablonskyi, D.; Nagaya, K.; Wada, S.; Mondal, S.; Tachibana, T.; et al. Radiation-Induced Chemical Dynamics in Ar Clusters Exposed to Strong X-ray Pulses. *Phys. Rev. Lett.* **2018**, *120*, 223201. [CrossRef]

17. Kumagai, Y.; Fukuzawa, H.; Motomura, K.; Iablonskyi, D.; Nagaya, K.; Wada, S.; Ito, Y.; Takanashi, T.; Sakakibara, Y.; You, D.; et al. Following the Birth of a Nanoplasma Produced by an Ultrashort Hard-X-ray Laser in Xenon Clusters. *Phys. Rev. X* **2018**, *8*, 031034. [CrossRef]
18. Rupp, D.; Flückiger, L.; Adolph, M.; Gorkhover, T.; Krikunova, M.; Müller, J.P.; Müller, M.; Oelze, T.; Ovcharenko, Y.; Röben, B.; et al. Recombination-Enhanced Surface Expansion of Clusters in Intense Soft X-ray Laser Pulses. *Phys. Rev. Lett.* **2016**, *117*, 153401. [CrossRef]
19. Bostedt, C.; Adolph, M.; Eremina, E.; Hoener, M.; Rupp, D.; Schorb S. Thomas, H.; De Castro, A.R.B.; Möller, T. Clusters in intense FLASH pulses: ultrafast ionization dynamics and electron emission studied with spectroscopic and scattering techniques. *J. Phys. B* **2010**, *43*, 194011. [CrossRef]
20. Bostedt, C.; Eremina, E.; Rupp, D.; Adolph, M.; Thomas, H.; Hoener, M.; De Castro, A.R.B.; Tiggesbäumker, J.; Meiwes-Broer, K.-H.; Laarmann, T.; et al. Ultrafast X-ray Scattering of Xenon Nanoparticles: Imaging Transient States of Matter. *Phys. Rev. Lett.* **2012**, *108*, 093401. [CrossRef]
21. Rupp, D.; Adolph, M.; Gorkhover, T.; Schorb, S.; Wolter, D.; Hartmann, R.; Kimmel, N.; Reich, C.; Feigl, T.; de Castro, A.R.B.; et al. Identification of twinned gas phase clusters by single-shot scattering with intense soft X-ray pulses. *New J. Phys.* **2012**, *14*, 055016. [CrossRef]
22. Gorkhover. T.; Adolph, M.; Rupp, D.; Schorb, S.; Epp, S.W.; Erk, B.; Foucar, L.; Hartmann, R.; Kimmel, N.; Kühnel, K.-U.; et al. Nanoplasma Dynamics of Single Large Xenon Clusters Irradiated with Superintense X-ray Pulses from the Linac Coherent Light Source Free-Electron Laser. *Phys. Rev. Lett.* **2012**, *108*, 245005. [CrossRef] [PubMed]
23. Rupp, D.; Adolph, D.; Flückiger, L.; Gorkhover, T.; Müller, J.P.; Müller, M.; Sauppe, M.; Wolter, D.; Schorb, S.; Treusch, R.; et al. Generation and structure of extremely large clusters in pulsed jets. *J. Chem. Phys.* **2014**, *141*, 044306. [CrossRef] [PubMed]
24. Gorkhover, T.; Schorb, S.; Coffee, R.; Adolph, M.; Foucar, L.; Rupp, D.; Aquila, A.; Bozek, J.D.; Epp, S.W.; Erk, B.; et al. Femtosecond and nanometre visualization of structural dynamics in superheated nanoparticles. *Nat. Photonics* **2016**, *10*, 93–97. [CrossRef]
25. Rupp, D.; Monserud, N.; Langbehn, B.; Sauppe, M.; Zimmermann, J.; Ovcharenko, Y.; Möller, T.; Frassetto, F.; Poletto, L.; Trabattoni, A.; et al. Coherent diffractive imaging of single helium nanodroplets with a high harmonic generation source. *Nat. Commun.* **2017**, *8*, 493. [CrossRef]
26. Langbehn, B.; Sander, K.; Ovcharenko, Y.; Peltz, C.; Clark, A.; Coreno, M.; Cucini, R.; Drabbels, M.; Finetti, P.; Di Fraia, M.; et al. Three-Dimensional Shapes of Spinning Helium Nanodroplets. *Phys. Rev. Lett.* **2018**, *121*, 255301. [CrossRef]
27. Schroedter, L.; Müller, M.; Kickermann, A.; Przystawik, A.; Toleikis, S.; Adolph, M.; Flückiger, L.; Gorkhover, T.; Nösel, L.; Krikunova, M.; et al. Hidden Charge States in Soft-X-ray Laser-Produced Nanoplasmas Revealed by Fluorescence Spectroscopy. *Phys. Rev. Lett.* **2014**, *112*, 183401. [CrossRef]
28. Iwayama, H.; Harries, J.R.; Shigemasa, E. Transient charge dynamics in argon-cluster nanoplasmas created by intense extreme-ultraviolet free-electron-laser irradiation. *Phys. Rev. A* **2015**, *91*, 021402. [CrossRef]
29. Saalmann, U.; Rost, J. Ionization of Clusters in Intense Laser Pulses through Collective Electron Dynamics. *Phys. Rev. Lett.* **2003**, *91*, 223401. [CrossRef]
30. Siedschlag, C.; Rost, J.-M. Small Rare-Gas Clusters in Soft X-ray Pulses. *Phys. Rev. Lett.* **2004**, *93*, 043402. [CrossRef]
31. Arbeiter, M.; Fennel, T. Rare-gas clusters in intense VUV, XUV and soft X-ray pulses: Signatures of the transition from nanoplasma-driven cluster expansion to Coulomb explosion in ion and electron spectra. *New J. Phys.* **2011**, *13*, 053022. [CrossRef]
32. Barke, I.; Hartmann, H.; Rupp, D.; Flückiger, L.; Sauppe, M.; Adolph, M.; Schorb, S.; Bostedt, C.; Treusch, R.; Peltz, C.; et al. The 3D-architecture of individual free silver nanoparticles captured by X-ray scattering. *Nat. Commun.* **2015**, *6*, 6187. [CrossRef] [PubMed]
33. Islam, M.R.; Saalmann, U.; Rost, J.M. Kinetic energy of ions after Coulomb explosion of clusters induced by an intense laser pulse. *Phys. Rev. A* **2006**, *73*, 041201. [CrossRef]
34. Thomas, H.; Bostedt, C.; Hoener, M.; Eremina, E.; Wabnitz, H.; Laarmann, T.; Plönjes, E.; Treusch, R.; de Castro, A.R.B.; Möller, T. Shell explosion and core expansion of xenon clusters irradiated with intense femtosecond soft X-ray pulses. *J. Phys. At. Mol. Opt. Phys.* **2009**, *42*, 134018. [CrossRef]

35. Chapman, H.N.; Fromme, P.; Barty, A.; White, T.A.; Kirian, R.A.; Aquila, A.; Hunter, M.S.; Schulz, J.; De Ponte, D.P.; Weierstall, U.; et al. Femtosecond X-ray protein nanocrystallography. *Nature* **2011**, *470*, 73–77. [CrossRef]
36. Seibert, M.M.; Ekeberg, T.; Maia, F.R.N.C.; Svenda, M.; Andreasson, J.; Jönsson, O.; Odić, D.; Iwan, B.; Rocker, A.; Westphal, D.; et al. Single mimivirus particles intercepted and imaged with an X-ray laser. *Nature* **2011**, *470*, 78–81. [CrossRef]
37. Neutze, R.; Wouts, R.; van der Spoel, D.; Weckert, E.; Hajdu, J. Potential for biomolecular imaging with femtosecond X-ray pulses. *Nature* **2000**, *406*, 752–757. [CrossRef]
38. Tono, K.; Togashi, T.; Inubushi, Y.; Sato, T.; Katayama, T.; Ogawa, K.; Ohashi, H.; Kimura, H.; Takahashi, S.; Takeshita, K.; et al. Beamline, experimental stations and photon beam diagnostics for the hard X-ray free electron laser of SACLA. *New J. Phys.* **2013**, *15*, 083035. [CrossRef]
39. Fukuzawa, H.; Nagaya, K.;Ueda, K. Advances in instrumentation for gas-phase spectroscopy and diffraction with short-wavelength free electron lasers. *Nucl. Inst. Methods Phys. Res. A* **2018**, *907*, pp.125–7. [CrossRef]
40. Kameshima, T.; Ono, S.; Kudo, T.; Ozaki, K.; Kirihara, Y.; Kobayashi, K; Inubushi, Y.; Yabashi, M.; Horigome, T.; Holland, A.; et al. Development of an X-ray pixel detector with multi-port charge-coupled device for X-ray free-electron laser experiments. *Rev. Sci. Instrum.* **2014**, *85*, 033110. [CrossRef]
41. Nishiyama, T.; Niozu, A.; Bostedt, C.; Ferguson, K.R.; Sato, Y.; Hutchison, C.; Nagaya, K.; Fukuzawa, H.; Motomura, K.; Wada, S.; et al. Refinement of single nanoparticles structure determination from low-quality single-shot coherent diffraction data. *IUCrJ*. under review. [CrossRef]
42. Als-Nielsen, J.; McMorrow, D. *Elements of Modern X-ray Physics*, 2nd ed.; John Wiley & Sons Ltd.: Chichester, UK, 2011; pp. 5–9.
43. Mie, G. Beiträge zur Optik trüber Medien, speziell kolloidaler Metallösungen. *Ann. Phys.* **1908**, *330*, 377–445. [CrossRef]
44. Hagena, O.F. Cluster ion sources (invited). *Rev. Sci. Instrum.* **1992**, *63*, 2374–2379. [CrossRef]
45. Dorchies, F.; Blasco, F.; Caillaud, T.; Stevefelt, J.; Stenz, C.; Boldarev, A.S.; Gasilov, V.A. Spatial distribution of cluster size and density in supersonic jets as targets for intense laser pulses. *Phys. Rev. A* **2003**, *68*, 023201. [CrossRef]
46. Vinko, S.M.; Ciricosta, O.; Wark, J.S. Density functional theory calculations of continuum lowering in strongly coupled plasmas. *Nat. Commun.* **2014**, *5*, 3533. [CrossRef] [PubMed]
47. SIMION®. Ion and Electron Optics Simulator. Available online: https://simion.com/ (accessed on 18 October 2019).